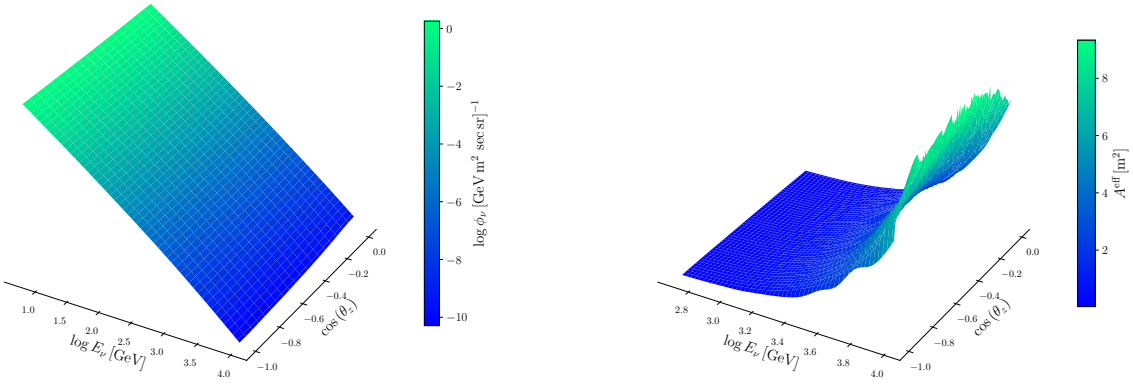

Fig. 0.1: Left panel: Interpolated South Pole atmospheric flux with data from [**?**]. *Right panel:* Interpolated IceCube effective area with data from [1].

0.1 Atmospheric neutrino flux

The flux comes from [**?**] The flux data is binned in $\cos(\theta_z^{true})$ and a selection is shown in Table 0.1. The fluxes are averaged over azimuthal direction and over solar minimum/maximum. The units of the fluxes are given as $\text{GeV}^{-1}\,\text{m}^{-2}\,\text{s}^{-1}\,\text{sr}^{-1}$ and are omitted from the table for clarity. We note that the fluxes for ν_τ and $\nu_{\bar{\tau}}$ are missing. This is due to the rapid decay (and hence, low flux) of the τ. Thus, we never have to use probabilities on the form $P_{\tau\beta}$, since we have no incoming atmospheric ν_τ flux.

Interpolating the data yields makes us capable of returning all four necessary fluxes for a given true energy and true zenith. The result is shown in Fig. .

E^{true} [GeV]	ϕ_μ	$\phi_{\bar{\mu}}$	ϕ_e	$\phi_{\bar{e}}$	$\cos(\theta_z^{true})_{min}$	$\cos(\theta_z^{true})_{max}$
27825	6.06×10^{-12}	3.17×10^{-12}	1.56×10^{-13}	1.04×10^{-13}	-0.2	-0.1
247707	5.94×10^{-16}	2.92×10^{-16}	1.36×10^{-17}	8.12×10^{-18}	-0.7	-0.6
22	3.33×10^{-2}	2.78×10^{-2}	9.57×10^{-3}	7.15×10^{-3}	-0.3	-0.2
432876	5.19×10^{-17}	2.32×10^{-17}	1.46×10^{-18}	9.83×10^{-19}	-1.1	-1.0
64280	1.58×10^{-13}	8.10×10^{-14}	3.49×10^{-15}	2.21×10^{-15}	-0.4	-0.3

Tab. 0.1: A selection of processed atmospheric South Pole fluxes from [**?**] by Honda et al. [**?**].

0.2 Event reconstruction

After an event has occurred, the IceCube algorithms process the data coming from the detector to *reconstruct* the event. This means that, given the parameters recorded by the detector, what are their "true" values? We are interested in two variables: the energy and the direction. Each event is tagged with a probable energy and zenith angle, called the recostructed parameters E^{reco} and $\cos(\theta_z^{reco})$, which are the parameters according to the DOMs. The collaboration then uses numerous sophisticated methods to backtrack the reconstructed parameters to the true parameters. So a charged lepton hits the DOMs, and we ultimately end up with the associated neutrino's true and reconstructed energy and zenith angle. The reconstructed parameters are what we are using to analyze the data (because this is what the detector actually sees), while the true

E^{true}_{min} [GeV]	E^{true}_{max} [GeV]	$\cos(\theta^{true}_z)_{min}$	$\cos(\theta^{true}_z)_{max}$	A^{eff} [m^2]
251	316	-0.92	-0.91	0.0174
794300	1000000	-0.80	-0.79	69.3600
3981	5012	-0.78	-0.77	3.1490
1585	1995	-0.07	-0.06	0.4659
398	501	-0.73	-0.72	0.0555

Tab. 0.2: IceCube effective area from [1]

pdg	E^{reco} [GeV]	$\cos(\theta^{reco}_z)$	E^{true} [GeV]	$\cos(\theta^{true}_z)$
13	1665	-0.645884	592	-0.653421
13	587	-0.373241	342	-0.424979
-13	1431	-0.177786	1169	-0.189949
-13	831	-0.807226	1071	-0.805559
13	988	-0.370746	1861	-0.367922

Tab. 0.3: A selection of the data found in **??**

parameters are used in the determination of that neutrino's "actual" flux and cross-section (because this is what nature sees).

How do we then translate between the reconstructed and true parameters? In this work, we are using two different methods, which are based on the form of data available to us.

0.3 IceCube event count

As the neutrinos have propagated the Earth, they arrive at the South Pole, where they interact in the ice to form their charged leptons. We now are interested in the effective area, i.e. the detector area that the lepton "sees". The effective area, A^{eff}, depends on several parameters, some of them being detector physical volume, E^{true},$\cos(\theta^{true}_z)$ and the neutrino cross-section. Fortunately, the binned A^{eff} is provided to us by the collaboration [1]. The data file has the following form

Here, A^{eff} has been averaged over A^{eff}_{μ} and $A^{\text{eff}}_{\bar{\mu}}$. Thus, it is not flavor dependent. Just as with the fluxes, we interpolate this in $E^{true}, \cos(\theta^{true}_z)$ and show the result

So now we have the physical quantities in the true parameters. But as we discussed, we need a way to translate this into the reconstructed parameters that the detector gives us. We will call the relationship between E^{reco} and E^{true} the energy resolution function, and the relationshop between $\cos(\theta^{reco}_z)$ and $\cos(\theta^{true}_z)$ the zenith resolution function. We assume the relationship to follow a logarithmic Gaussian distribution, giving it the form

$$R(x^r, x^t) = \frac{1}{\sqrt{2\pi}\sigma_{x^r} x^r} \exp\left[-\frac{(\log x^r - \mu(x^t))^2}{2\sigma^2_{x^r}}\right] . \tag{0.1}$$

The parameters of the Gaussian are $\sigma_{x^r}(x^t)$ and $\mu(x^t)$, which are functions of the true parameters. By multiplying the Gaussian in Eq. 0.1, we are reweighing the values by the probability density of that point. This process is also called *smearing* because it effectively spreads out the data around a certain point.

So how do we then obtain $\sigma_{x^r}(x^t)$ and $\mu(x^t)$ needed to construct the Gaussian? A Monte Carlo sample publically released by the collaboration has all the ingredients that we need [2]. In Table. 0.3 we show a selection of the data. The "pdg" column refers to the Monte Carlo particle classification, where 13 is the tag for ν_μ, while -13 refers to an $\bar{\nu}_\mu$. Here we note a crucial property of the IceCube dataset that will impact our analysis: the MC released by the collaboration only includes simulated muon events.

First, we let $\cos(\theta^{reco}_z) = \cos(\theta^{true}_z)$ for all values. The angular resolution in IceCube for track-like events is less than 2°, making $\cos(\theta^{true}_z)$ coincide with $\cos(\theta^{reco}_z)$ for our study [3]. Thus, we only need to concern ourselves with the energy resolution. In Fig. 0.3, we have plotted all event counts found in the MC file, over 8 million. However, this is too much data to process efficiently, with many outliers that ultimately don't weigh in that much in the final event count. To resolve this, we have opted to train a Gaussian process regressor on the dataset, from which we can extract the predicted mean and standard deviation for a point. When doing this over E^{reco}, we sample E^{true} in the 99%th percentile around the predicted mean. We then obtain the shaded band shown in Fig. 0.3.

The event rate for each bin reads

$$N_{ij} = T \int_{(\cos\theta^r_z)_i}^{(\cos\theta^r_z)_{i+1}} \mathrm{d}\cos\theta^r_z \int_{E^r_j}^{E^r_{j+1}} \mathrm{d}E^r \int_0^{\pi} R(\theta^r, \theta^t)\mathrm{d}\cos\theta^t \int_0^{\infty} R(E^r, E^t)\mathrm{d}E^t \times \left[\sum_\beta \phi^{\text{det}}_\beta A^{\text{eff}}_\beta\right] , \tag{0.2}$$

where T is the live time of the detector.

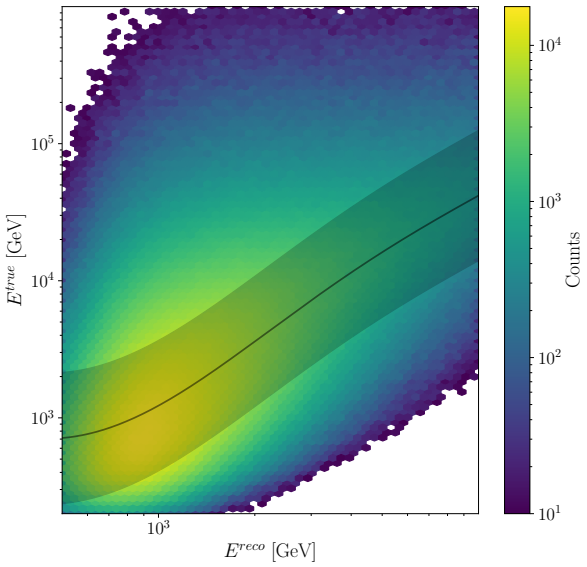

Fig. 0.2: Relationship between the true and reconstructed muon energy in the IceCube MC sample [2] . Shaded area shows the 99.9th percentile limits predicted by the regressor trained on this set.

BIBLIOGRAPHY

[1] IceCube Collaboration.

[2] IceCube Collaboration.

[3] Aartsen, M. G., Abbasi, R., Ackermann, M., Adams, J., Aguilar, J. A., Ahlers, M., Ahrens, M., Alispach, C., Amin, N. M., Andeen, K., Anderson, T., Ansseau, I., Anton, G., Argüelles, C., Auffenberg, J., Axani, S., Bagherpour, H., Bai, X., Balagopal V., A., Barbano, A., Barwick, S. W., Bastian, B., Basu, V., Baum, V., Baur, S., Bay, R., Beatty, J. J., Becker, K.-H., Becker Tjus, J., BenZvi, S., Berley, D., Bernardini, E., Besson, D. Z., Binder, G., Bindig, D., Blaufuss, E., Blot, S., Bohm, C., Böser, S., Botner, O., Böttcher, J., Bourbeau, E., Bourbeau, J., Bradascio, F., Braun, J., Bron, S., Brostean-Kaiser, J., Burgman, A., Buscher, J., Busse, R. S., Carver, T., Chen, C., Cheung, E., Chirkin, D., Choi, S., Clark, B. A., Clark, K., Classen, L., Coleman, A., Collin, G. H., Conrad, J. M., Coppin, P., Correa, P., Cowen, D. F., Cross, R., Dave, P., De Clercq, C., DeLaunay, J. J., Dembinski, H., Deoskar, K., De Ridder, S., Desai, A., Desiati, P., de Vries, K. D., de Wasseige, G., de With, M., DeYoung, T., Dharani, S., Diaz, A., Díaz-Vélez, J. C., Dujmovic, H., Dunkman, M., DuVernois, M. A., Dvorak, E., Ehrhardt, T., Eller, P., Engel, R., Evenson, P. A., Fahey, S., Fazely, A. R., Fedynitch, A., Felde, J., Fienberg, A. T., Filimonov, K., Finley, C., Fox, D., Franckowiak, A., Friedman, E., Fritz, A., Gaisser, T. K., Gallagher, J., Ganster, E., Garrappa, S., Gerhardt, L., Glauch, T., Glüsenkamp, T., Goldschmidt, A., Gonzalez, J. G., Grant, D., Grégoire, T., Griffith, Z., Griswold, S., Günder, M., Gündüz, M., Haack, C., Hallgren, A., Halliday, R., Halve, L., Halzen, F., Hanson, K., Hardin, J., Haungs, A., Hauser, S., Hebecker, D., Heereman, D., Heix, P., Helbing, K., Hellauer, R., Henningsen, F., Hickford, S., Hignight, J., Hill, G. C., Hoffman, K. D., Hoffmann, R., Hoinka, T., Hokanson-Fasig, B., Hoshina, K., Huang, F., Huber, M., Huber, T., Hultqvist, K., Hünnefeld, M., Hussain, R., In, S., Iovine, N., Ishihara, A., Jansson, M., Japaridze, G. S., Jeong, M., Jones, B. J. P., Jonske, F., Joppe, R., Kang, D., Kang, W., Kappes, A., Kappesser, D., Karg, T., Karl, M., Karle, A., Katz, U., Kauer, M., Kellermann, M., Kelley, J. L., Kheirandish, A., Kim, J., Kintscher, T., Kiryluk, J., Kittler, T., Klein, S. R., Koirala, R., Kolanoski, H., Köpke, L., Kopper, C., Kopper, S., Koskinen, D. J., Koundal, P., Kowalski, M., Krings, K., Krückl, G., Kulacz, N., Kurahashi, N., Kyriacou, A., Lanfranchi, J. L., Larson, M. J., Lauber, F., Lazar, J. P., Leonard, K., Leszczyńska, A., Li, Y., Liu, Q. R., Lohfink, E., Lozano Mariscal, C. J., Lu, L., Lucarelli, F., Ludwig, A., Lünemann, J., Luszczak, W., Lyu, Y., Ma, W. Y., Madsen, J., Maggi, G., Mahn, K. B. M., Makino, Y., Mallik, P., Mancina, S., Mariş, I. C., Maruyama, R., Mase, K., Maunu, R., McNally, F., Meagher, K., Medici, M., Medina, A., Meier, M., Meighen-Berger, S., Merz, J., Meures, T., Micallef, J., Mockler, D., Momenté, G., Montaruli, T., Moore, R. W., Morse, R., Moulai, M., Muth, P., Nagai, R., Naumann, U., Neer, G., Nguyen, L. V., Niederhausen, H., Nisa, M. U., Nowicki, S. C., Nygren, D. R., Obertacke Pollmann, A., Oehler, M., Olivas, A., O'Murchadha, A., O'Sullivan, E., Palczewski, T., Pandya, H., Pankova, D. V., Park, N., Parker, G. K., Paudel, E. N., Peiffer, P., Pérez de los Heros, C., Philippen, S., Pieloth, D., Pieper, S., Pinat, E., Pizzuto, A., Plum, M., Popovych, Y., Porcelli, A., Prado Rodriguez, M., Price, P. B., Przybylski, G. T., Raab, C., Raissi, A., Rameez, M., Rauch, L., Rawlins, K., Rea, I. C., Rehman, A., Reimann, R., Relethford, B., Renschler, M., Renzi, G., Resconi, E., Rhode, W., Richman, M., Riedel, B., Robertson, S., Rongen, M., Rott, C., Ruhe, T., Ryckbosch, D., Rysewyk Cantu, D., Safa, I., Sanchez Herrera, S. E., Sandrock, A., Sandroos, J., Santander, M., Sarkar, S., Sarkar, S., Satalecka, K., Scharf, M., Schaufel, M., Schieler, H., Schlunder, P., Schmidt, T., Schneider, A., Schneider, J., Schröder, F. G., Schumacher, L., Sclafani, S., Seckel, D., Seunarine, S., Shefali, S., Silva, M., Smithers, B., Snihur, R., Soedingrekso, J., Soldin, D., Song, M., Spiczak, G. M., Spiering, C., Stachurska, J., Stamatikos, M., Stanev, T., Stein, R., Stettner, J., Steuer, A., Stezelberger, T., Stokstad, R. G., Stößl, A., Strotjohann, N. L., Stürwald, T., Stuttard, T., Sullivan, G. W., Taboada, I., Tenholt, F., Ter-Antonyan, S., Terliuk, A., Tilav, S., Tollefson, K., Tomankova, L., Tönnis, C., Toscano, S., Tosi, D., Trettin, A., Tselengidou, M., Tung, C. F., Turcati, A., Turcotte, R., Turley, C. F., Ty, B., Unger, E., Unland Elorrieta, M. A., Usner, M., Vandenbroucke, J., Van Driessche, W., van Eijk, D., van Eijndhoven, N., Vannerom, D., van Santen, J., Verpoest, S., Vraeghe, M., Walck, C., Wallace, A., Wallraff, M., Watson, T. B., Weaver, C., Weindl, A., Weiss, M. J., Weldert, J., Wendt, C., Werthebach, J., Whelan, B. J., Whitehorn, N., Wiebe, K., Wiebusch, C. H., Williams, D. R., Wills, L., Wolf, M., Wood, T. R., Woschnagg, K., Wrede, G., Wulff, J., Xu, X. W., Xu, Y., Yanez, J. P., Yodh, G., Yoshida, S., Yuan, T., Zhang, Z., Zöcklein, M., and IceCube Collaboration. **102**(5), 052009.